Quantitative atomic force microscopy measurements of *Acinetobacter* morphology

C. Phoebe Lostroh (plostroh@coloradocollege.edu)
Colorado College https://orcid.org/0000-0002-7956-9536
Caroline M. Boyd
Colorado College
Nicholas Lammers
Colorado College
Kaleb S. Roush
Colorado College
Sara L. Worsham
Colorado College
Saúl Maravilla
Colorado College
Anis Buttar-Miller
colorado college
Kristine M. Lang
Colorado College

Research article

Keywords: Acinetobacter baylyi, atomic force microscopy, minC mutant, morphology

Posted Date: January 13th, 2020

DOI: https://doi.org/10.21203/rs.2.20752/v1

Abstract

Acinetobacter baylyi are variously reported as spherical or rod-shaped. Here we use atomic force microscopy (AFM) to make quantitative nanometer-scale measurements of cellular length and width for thousands of individual cells. We quantify the heterogeneity of populations grown in varying environmental conditions that dramatically affect cell shape. In particular, we look at morphology changes across a growth curve, and we examine cells from populations grown in various growth media. We also examine the morphology of a *minC* mutant, which suggests an interpretation for the morphological types observed in wild type cells.

Introduction

Most bacterial cells can be characterized as rod-shaped, coccoid, or spiral, although there are exceptions (1). Rod-shaped cells can have different aspect ratios so that some appear long and thin, while others are termed coccobacillary because their length is only slightly longer than their width. Bacterial morphology is critical for survival because it contributes to essential parameters such as overall cell size and surface area-to-volume (SA:V) ratio (2). We study Acinetobacter as a model for bacteria that can change shape in response to environmental cues.

Acinetobacter species are ubiquitous in soils and known for their ability to use diverse carbon sources and to be naturally transformable (3). A. baylyi strain ADP1 is a well-studied derivative of a strain termed BD413, which was itself a microencapsulated derivative of BD4 (4). Strain BD4 was isolated from soil using minimal medium with meso 2,3-butanediol as the sole carbon source (5, 6). Like other Acinetobacter spp., ADP1 exhibits catabolic versatility, able to use diverse substrates such as alkanesulfonates, p-Hydroxybenzoate, catechol, and salicylate esters (to name a few; reviewed in (3, 7)). This versatility likely enables survival in highly competitive soil environments.

Images of Acinetobacter reveal cells that sometimes have an aspect ratio (length:width) similar to that of Escherichia coli, and other times have a nearly coccoid appearance, even for the same species. For example, light images of A. baylyi often show typical short rod morphology, but the original description of the same cells shows them as much more coccoid (4, 8). During routine use of a light microscope we also noticed that the cells sometimes had different aspect ratios. Thus, we decided to investigate the size and shape of the cells using atomic force microscopy (AFM). We sampled A. baylyi at different times over a typical growth curve in general purpose media containing 1% tryptone, 0.5% yeast extract, and 0.5% NaCl, and then analyzed the features of thousands of cells selected at random. To our knowledge, this is the first publication investigating A. baylyi using AFM, and one of the only AFM studies characterizing the size, shape, and morphology of bacteria over the course of a growth curve.

Atomic force microscopy is an increasingly useful technique for microbiologists (9–13). The strength of AFM exploited in this study is that it enables quantitative nanometer-scale measurements of cellular length and width for individual cells and from these measurements, other cellular parameters such as

surface area to volume may be calculated for each cell (14, 15). We performed these measurements on cells grown under varying environmental conditions, and we see that growth conditions dramatically affect cell shape. In particular, we look at morphology changes across an entire growth curve from exponential to stationary phase, and we examine cells from populations grown in different growth media.

Results

Cellular morphology changes during a growth curve

Figure 1. AFM topographs displaying bacterial morphological changes during a growth curve. All images are 15 μm x 15 μm and were obtained at population age A) 2 hours, B) 4 hours, C) 6 hours, D) 8 hours and E) 11 hours after inoculation. The only image post-processing performed was a simple first order plane fit. The boxed cells in each image are described in the text and presented in Fig. 4 in three-dimensional close-ups. Panel F shows cross-sections from panels A and C in the upper and lower graphs respectively. These cross-sections demonstrate the three-dimensional nature of AFM data and illustrate how cell length is measured. The star on an image and its corresponding cross-section are at about the same position. For the upper graph in Panel F, the cell length is defined as the distance between the two local minima at the cell's end, as marked by the dashed lines, yielding a length of 1.14 μm for this cell. For the lower graph in Panel F, the local minima differ significantly in height, so here the cell length is defined as the distance between the shallowest local minimum and the equal height location on the opposite side of the cell, as marked by the dashed lines, yielding a length of 2.14 μm.

Both within and between the images, the panels in Fig. 1 show a striking amount of morphological heterogeneity. Cells from all time points (Panels A-E) contain both round and rod-shaped cells, while cells from later times also contain filaments (Panels C and E), with a particularly long filament boxed in Panel E. In addition, there is a striking amount of heterogeneity among the surface features of the cells. Some cells are smooth across their top surface (see boxed cell in bottom center of A), while some have small indentations towards their poles (see boxed cells at bottom left of C). Some cells appear sunken in throughout their centers (see boxed cells in D), while some cells are asymmetrically sunken at their midline (see boxed cells in B). Other species of bacteria also have some of these features when imaged with AFM (14, 16–21).

The growth curve corresponding to Fig. 1 is given in Fig. 2D, with the growth rate given in 2E. These figures show that the population is in exponential phase from 2–5 hours after inoculation. A transition from exponential to stationary phase occurs from 5–7 hours after inoculation, during which time the population is still increasing, but at a decreasing rate. Stationary phase begins 7 hours after inoculation at which time the growth rate is close to zero and remains that way going forward. Vertical gray lines on Fig. 2 delineate these three time periods.

Figure 1 shows a clear progression of shape from one panel to the next as cells go through the growth phases identified in Fig. 2D and E. Panels 1A and B, taken of exponential phase cells, show spherical

cells, coccobacilli, and short rods. During the exponential to stationary phase transition at 6 hours after inoculation, the cells become longer rods as shown in panel C, and many septa are observed, an example of which is boxed at the left middle of the panel. In panels D and E, which derive from stationary phase proper, we see a decidedly narrower population of primarily rods.

In short, Fig. 1 illustrates an array of morphological heterogeneity that underlies the growth curves of Fig. 2D. To investigate further the interrelationship between morphology and growth phase, we quantified and categorized cellular size and morphology as described in the following paragraphs.

Atomic force microscopy imaging and quantification

Atomic force microscopy (AFM) is a tool well suited to studying bacterial shape (10, 11, 13). Its resolution is limited by the sharpness of the tip of the cantilever used to take the image, which is typically of order 10 nm. Since usual bacterial dimensions are of order 1 μm, AFM can easily resolve small changes in bacterial shape. In addition, AFM produces true three-dimensional images as shown in Fig. 1F, which shows a cross section of cells from panels 1A and 1C. Finally, preparing cells for AFM imaging is straightforward.

To make a series of images as in Fig. 1, we sample a single culture at regular intervals to make samples and then image by AFM (see Methods for details). To quantify cell size, we image each sample in several disparate locations to ensure we see its full diversity. For each of the resulting images, we randomly choose 50 cells. For each cell, we measure its length and width and classify it according to its surface features. Figure 1F shows how individual cell measurements are made using a cross-section from 1A and 1C. In brief, we simultaneously use a cross-section and its corresponding image to locate the local minima that define the edges of the cells (as indicated by vertical dashed lines on the cross-sections). The distance between the minima is defined as the length or width, with length always the larger of the two distances.

Using thousands of individual cells' measurements, in Fig. 2A, B and C we plot the progression of bacterial shape as a function of time since inoculation. All the data in these panels comes from a single time series, but the same morphological trends were evident in other independent time series. For the time series data presented in Fig. 2 we assessed three to four 30 μm X 30 ∝m images per hour, taken on the hour starting 2 hours and finishing 12 hours after the inoculation of the broth, for a total of 38 images and 1900 cells assessed. With this data in hand, we are now in a position to look quantitatively at the morphological trends underlying the growth curve.

Interrelationship of growth curve and morphology changes

Figure 2A, B, and C show the changes of the average (red circles), median (black squares), and distribution (gray bars) of cell measurements during the growth curve shown in 2D with corresponding growth rate shown in 2E.

We focus first on cell length in Fig. 2A. The average length of the population is 1.91 μm for cells in exponential phase, defined to be from 2–4 hours after inoculation. In hour 5 just as the growth rate begins to decline, there is a rapid increase in average cell length. The average length for cells 5–7 hours after inoculation is 2.65 μm, so this represents a 39% increase in length over exponential phase cells. In addition, there is a diversification of lengths indicated by a doubling in size of the cell-length distribution gray bars. This diversification can be seen in more detail in the histogram of lengths shown in Fig. 3. Comparison of the distribution of length in exponential phase (Fig. 3G) to the distribution of length in the transition time (Fig. 3H) shows that for cells in exponential phase the distribution is bell shaped with weight approximately between 1.0 and 2.5 μm and small number of cells in the higher length tail, whereas for cells in transition, the histogram has shifted to being fairly flat between 1.0 and 3.4 μm.

Returning to Fig. 2A, during the transition, the average cell length remains high and highly diversified as the growth rate falls through hour 7. In stationary phase starting in hour 8 and persisting through hour 12, the average cell length falls to 1.75 μm, similar to exponential phase cells. Likewise, a comparison of the length histograms in Fig. 3G, H and I shows that the distribution in stationary phase resembles that of exponential phase, being bell shaped with weight approximately between 1.0 and 2.5 um.

We now consider the changes in cell width in Fig. 2B. In hours 2–4 in exponential phase cell width averages 1.13 μm. Cell width remains at about this value even as the growth rate begins to fall in hours 5 and 6. In hour 7, just as the growth rate reaches zero and stationary phase begins, the average width begins to decrease, settling in hour 8 and beyond at an average value of 0.87 μm which is 30% lower than its exponential phase value.

Using individual cell lengths and widths, it is possible to calculate the surface area to volume (SA/V) ratio for each cell and hence the average SA/V for all cells at a given time point. The changes in surface area to volume (SA/V) ratio are given in Fig. 2C. In hour 2–4 in exponential phase the average SA/V is 4.68 μm^{-1}. It drops in hour 5 due to the dramatic increase in cell lengths, and then between hours 5–8 during the transition from exponential to stationary phase, SA/V increases steadily. In stationary phase proper in hour 8 and beyond, the SA/V ratio settles in at an average value of 5.91 μm^{-1} which is 26% higher than its exponential phase value.

In Fig. 3 we consider how the width and surface area to volume of cells vary with their length in the three time periods during the growth curve. To make this figure, we use cell length to bin all the cells in a given time period. For each length bin, we plot the average width (Fig. 3ABC) and the average surface area to volume (Fig. 3DEF). Figure 3GHI gives the counts for each length bin. Since cells lengthen as they age in preparation for cell division, it is useful to think of the horizontal axis of the plot as indicating increasing cell age.

From Fig. 3A, cells in exponential phase with lengths less than about 2.1 μm (vertical dashed line) are narrow with the width increasing as cells get longer. Cells with lengths longer than 2.10 μm have a more constant width with an average of 1.20 μm (horizontal dashed line). The trends for width vs. length are

similar for cells in transition (3B) and stationary phase (3C); however, the average width approached decreases to 1.10 μm and 0.92 μm respectively for lengths longer than 2.10 μm and 1.60 μm in transition and stationary phase respectively. Note that for stationary phase, the asymptotic width is reached at a shorter length than in exponential phase or transition.

We now consider the SA/V as a function of length as shown in Fig. 3D, E and F. In exponential phase and during transition the SA/V is decreasing for lengths less than about 2.1 μm (vertical dashed line), whereas above 2.10 μm it reaches an asymptotic average value of 4.09 μm^{-1} and 4.30 μm^{-1} respectively. In stationary phase, the SA/V is decreasing at all lengths with a definitive inflection point at a length of about 1.6 μm. As was also see in Fig. 2C, the SA/V is higher in stationary phase than during the other two time periods. Indeed, the SA/V in stationary phase never reaches the asymptotic values seen in exponential and transition time periods.

We finish this section on cell dimensions by examining the characteristic that is perhaps most obvious when cells are imaged- their shape, or to be more precise the ratio of their length to their width. In Fig. 4, we plot the fraction of cells that would be perceived as spherical, intermediate, and as rods during each of the periods identified in the growth curve of Fig. 2. We find that the distribution of shapes changes between the periods. In exponential phase, we see the highest fraction of spherical cells for any period at 20% and also the highest fraction of intermediate cells at 43%, whereas rods comprise only 37%. This is the quantification of the visual perception that Fig. 1A is dominated by round and short fat rod cells. During the transition, the fraction of spherical cells is less than a third, and the fraction of intermediate cells is less than half of what they were earlier. Instead rods are by far the dominant shape comprising 74% of the population. This dominance of rods in transition is clearly evident in the visual perception of Fig. 1C. Finally, in stationary phase, the distribution of shapes rebounds back toward the exponential distribution, in that the fraction of spherical and intermediate cells increases at the expense of the rods. However, rods are the dominant shape during this period at 56%, as seen in Fig. 1D and 1E. The morphological changes quantified in this figure explain why previous descriptions of A. baylyi vary in the literature (4, 8).

Cell surface topography

After studying thousands of cells in images such as those shown in Fig. 1, we identified five distinctive cell surface morphologies we designate as bite, divot, canoe, smooth and filament. These types are shown in Fig. 5A. All of the close-ups in Fig. 5 are taken from the larger images presented in Fig. 1 so that their context can be observed. For each cell type we created a stringent quantitative definition of its morphology as detailed in the Methods. We used these definitions to classify every cell measured. Brief descriptions of the cell types are as follows.

Bite cells are characterized by a single deep, relatively steep-sided indentation that occurs midway along the cell's long axis. This indentation can be bilaterally symmetric or not- an example of each is shown. Divot cells are characterized by a pair of small depressions occurring near the cell's poles. A cross section

of a divot cell appears in Fig. 1F (lower graph) with the divots marked by arrows. Canoe cells have central surface depression circumscribed by a higher, continuous ridge along the cell edge. A cross-section of a canoe cell appears in Fig. 1F (upper graph) with the center of the canoe marked by an arrow. Smooth cells are featureless with minimal elevation changes on their surface. Filaments are all cells with length greater than 4 μm regardless of any surface features. Filaments may have surface features like those previously described, as in this case a canoe, but if sufficiently long will be classified as a filament.

In addition to classifying cells into the morphological categories shown in Fig. 5A, we also observe cells that have clear septa at their midlines as shown in Fig. 5B. As detailed in the Methods, a septating cell is defined as one whose width at the septum is 50%-90% of its full width. Surface features on septating cells indicate these cells are septating, rather than two cells of that type. For example, in the septating canoe cell shown, the high continuous ridge along the cell edge dips at the septum, and in the septating divot cell there are divots only at the extreme poles of the cell. For all cells measured, we noted whether such septa were present, and created a separate overlaid classification of cells as septating.

Using the strict definitions detailed in the methods, 62% of the total cells measured fall into one of the five cell types shown in Fig. 5A. The remaining cells had surface features that were a combination of one of the types shown or were simply too irregular to classify using our strict definitions. Many published AFM images of bacterial cells show the kinds of surface features seen in Fig. 5 (14, 16–19), including A. baumannii (20, 21).

Figure 6. Relative frequency of occurrence for cell types over a growth curve. The upper graph shows the relative frequency of occurrence for the five cell types identified in Fig. 5A during exponential phase (hours 2–4 after inoculation), the transition (hours 5–7), and stationary phase (hours 8–12). The lower panel gives the percentage of cells observed to be septating during those same three time periods.

In Fig. 7, we look at the average length, width and SA/V of the cell types over the growth curve. Focusing first on the horizontal axis of the figure, we look at length variation. In exponential phase, smooth and bite cells have much same average length, whereas canoe cells are shorter. Divot cells are longer than either of the three types and septating cells are the longest. During the transition, all the cells have shifted being longer, and each cell type is longer than its respective type was exponential phase. Nonetheless, the relative size relationships among the types still holds. Smooth, bites and canoes are the shortest cells, divots are longer, and septating cells are the longest of all. In stationary phase, cells shift back to shorter lengths, and again all cell types are shorter than their respective types during the transition. For the third time, the same trends hold regarding the relative lengths of the cell types.

We now focus on the vertical axis of Fig. 7 to examine trends in the width of cell types. In exponential phase, canoes and smooth cells have similar widths with bites a bit narrower, whereas divots and septating cells are wider. During the transition from exponential phase to stationary phase, all the cell types have narrower widths. Bites and smooth cells have similar widths, again with divots and septating cells wider. However, now the canoes are very narrow as compared to all other cells during this time. In stationary phase, all the cell types have again shifted to lower widths. A similar pattern holds regarding

the relationships between cell types- bites, smooth and canoes are the narrowest cells, with divots and septating cells wider.

On Fig. 7 we also plot SA/V ratio as the colored background behind the graph, and the lines show curves of constant SA/V for a cell assuming it is a rod with a hemispherical end cap. For this geometry, the SA/V will increase if a cell becomes either shorter or narrower. From this we observe that cells in exponential phase, which have about the same lengths as those in stationary phase, have nonetheless much lower SA/V because they are wider. We take an example of canoes which have almost the same length in the two phases. Nonetheless, in exponential phase the average SA/V is 4.63 μm^{-1}. whereas in stationary phase the SA/V is 5.78 μm^{-1}, an increase by a factor of 25% which is almost entirely mediated by changes in width.

Cell division mutant

In reading the literature we were struck by the resemblance between our bite cells and cell division mutant Escherichia coli cells (22, 23). To explore this resemblance, we imaged minC mutants of A. baylyi during exponential phase. The results are shown in Fig. 8.

Figure 8A shows that the minC mutant consists mostly of filamented cells, as expected because minicells likely wash away during sample preparation. Along the length of these filaments are indentations that can be compared to those observed in wild type cells shown in Fig. 1B. Zooming in on the boxed cell in Fig. 8A, in Fig. 8B we show a close-up of the one of the indentations, which can be compared to the close-up bite cells in Fig. 5A.

Cellular morphology in varying culture media

Changes in cellular morphology during different phases of a typical growth curve in general purpose media were presented in Figs. 1–7. In this section we present morphology data from exponential phase cells grown in varying culture media. The data presented in this section will allow us to draw comparisons between cells in various growth stages and cells growing in media of varying nutritional value.

To this end, we grew cells in each of the following media: lysogeny broth (LB), lysogeny broth supplemented with ethanol (LE) or glucose (LG), or minimal media with ethanol (ME), glucose (MG), or 2–3 butanediol (MB) as carbon sources. These six media were selected to attempt to provide the most variable growth rates achievable in < 24 hours of growth in a flask. 2–3 butanediol is also of historical interest because it was used in the enrichment that led to the isolation of A. baylyi strain BD4 (6).

For each medium, we made samples of exponential phase cells from four biological replicates, and we used AFM to image each sample. To quantify the images, we measured the length and width of ~ 75 cells in each of the four images for each of the six media, for a total of 1900 cells assessed. In addition, we took growth curves to find the doubling time for cells in that medium. These data are used to generate the graphs shown in Fig. 9.

From Fig. 9, we make the following observations. The doubling time for all cells grown in LB independent of the additive is about the same. In addition, for all cells grown in LB the length (Panel A), width (Panel B), and SA/V ratios (Panel C) do not substantively differ with differing additive. A comparison between Fig. 9 and Fig. 2 shows that the average length, width and SA/V of cells grown in LB + any additive is in the same range as exponential phase cells in Fig. 2, which were grown in LB.

For the cells grown in minimal media the story is quite different. In this case, the doubling time varies substantially with the additive. As seen in Fig. 9, cells with longer doubling times are substantially shorter (Panel A) and narrower (Panel B), which means they have consequently higher SA/V ratios (Panel C). We obtain an estimate for how size changes with doubling time by fitting the three minimal media points in each of the panels of Fig. 9. From this we find that length decreases at a rate of 0.47 μm/doubling time hour, the width decreases at a rate of 0.12 μm/hour, and the SA/V increases at a rate of 1.06 μm^{-1}/hour.

In Fig. 10 we show a typical image of cells having the highest doubling time and smallest average size, those grown in minimal media with added glucose. A visual comparison between Fig. 10 and Fig. 1A (both 15 μm images) yields a visceral impression for the size difference.

In addition to changing cell size, changing the additive in the growth medium changes cell shape as shown in Fig. 11. Cells grown in ME have a similar shape distribution to cells grown in LB during exponential phase (compare to Fig. 4). For the cells with increasing doubling times, those grown in MB and MG, the fraction of non-rod shapes increases steadily, so that for MG almost all cells are spherical or intermediate. Clearly Acinetobacter baylyi cells alter their aspect ratios depending on the broth used for growth, which could account for some of the variation in reports of their shape in the literature (6, 7, 24, 25).

Discussion

Acinetobacter cells control their width to alter SA/V and adapt to changing conditions

A higher SA/V ratio enhances a cell's ability to acquire adequate nutrition or release adequate waste products because it increases the relative area available for transport of nutrients and waste while decreasing the amount of cytoplasm (26). For the size and geometry of our cells, their SA/V will increase if a cell becomes either shorter or narrower. Thus, in response to stressful environmental conditions, we might expect cells to become shorter and/or narrower. In the case of Acinetobacter, it appears that cells decrease their width, and hence increase their SA/V ratio, in response to environmentally stressful situations. We observe this in several situations.

In the experiment whose results are displayed in Fig. 9, we looked at exponential phase cells grown in media with varying carbon sources. Panel 9B shows that as the doubling time increases, cells become increasingly narrow. This narrowing in turn increases their SA/V.

We can make the same observation if we look at the changes in the width of cells over a growth curve. In Fig. 7, we see that exponential phase cells (green) are on average wider than transition cells (black), which are in turn wider than stationary phase cells (white). The statement above holds for any individual cell type as well as the average of all cells. So as environmental conditions deteriorate at the end of exponential phase leading to the transition to stationary phase, cells become progressively narrower, thereby increasing their SA/V ratio.

The phenotype of minC mutants suggests an interpretation for the observed topogrophies

As expected, the minC Acinetobacter mutant is filamented. The highly-conserved MinC protein is essential for positioning the septum because it is needed to localize the Z ring (27). Interestingly, we observed indentations all along the lengths of the filamented minC deficient mutants (Fig. 8); the indentations quantitatively resemble the bite structures found at mid-cell in the wild type cells (Figs. 1B and 5A). In contrast, in the minC mutant, the bite structures appear at varying locations along the long axis of the filamented cell and not exclusively at the center of cell unit-size chunks of the filaments. Perhaps when the minC filaments, which contain many incomplete divisomes, dry prior to imaging, the cell wall collapses above the incomplete divisomes. The result is a bite structure. These observations raise the possibility that the bite structure in wild type cells results from a partially-constructed divisome as follows.

Long septating cells appear similar to two newborn canoe cells that are still connected, as seen in Fig. 5A. Second, canoe cells are about half the length of septating cells; for example, in exponential phase, the ratio of canoe length to septating length is 0.52. Therefore, canoe cells are probably the youngest newborn cells in the wild type populations. Bite type cells are usually a little bit longer and characterized by a single deep, relatively steep-sided indentation that occurs midway along the cell's long axis. This position coincides with the position of the future divisome in young cells. If a divisome were partially constructed, as it is in both filamented minC filaments and in young wild type cells, this could lead to the partial collapse of the cell wall upon dehydration. Divot cells are longer than bite cells, and so they are probably older. As seen in Fig. 5A, divot cells have a raised section at the cell center (28, 29). Perhaps because they have grown for a longer period of time since cell division occurred, they have constructed a more complete divisome near their midline. The symmetrical divot appearance could reflect the fact that the central divisome is a robust structure that consists of many different proteins completely encircling the midline of the cell (28). The short canoe cells may have completely indented middles because they had not yet begun the process of building a divisome.

In summary, we suggest that cell types represent steps in the cell growth and division process: canoes are newborn cells, which in due time will become bite cells as the cell division process continues. Next ,as the divisome matures, divot cells become septating cells, which are clearly in the process of dividing. These indented cell types have been observed in other AFM studies of bacteria over many years (14, 16–19, 21).

Progression of width during a division cycle

The width of cells varies in a consistent pattern during a division cycle as seen in Fig. 7. Within each of the three growth phases, canoes and bites are narrower than divot and septating cells during that same period. Because canoes and bites are younger (shorter), it appears that recently divided cells are more narrow than older cells.

This same trend can also be inferred looking at the data in Fig. 3. As shown in 3A, 3B and 3C, shorter and younger cells are narrower for all time periods of the growth curve. Cells widen as they lengthen and age until they reach a saturation width. They remain at this saturation width until they divide to become young narrow cells again. The saturation width is different during different phases of a growth curve.

Cellular changes during a growth curve

Starting in exponential phase, Fig. 2 shows us that the cell population as whole has an average length of 1.91 μm and is relatively wide at 1.13 μm. These cell dimensions give a relatively low SA/V value during this time period when cells have optimal environmental conditions. Figure 6 shows that almost half of the population in exponential phase consists of bite cells, which is also consistent with cells in exponential phase dividing frequently. The ratio of the width of septating cells to the width of canoe cells is 1.02, indicating that during conditions of abundance, canoes and septating cells are almost the same width (Fig. 7).

As the transition from exponential phase to stationary phase begins in hour five, Fig. 2E shows the growth rate begins to decline. At that same time, several things happen in the population. First, the fraction of bite cells declines and the fraction of divot cells increases (Fig. 6, upper graph). Second, the number of septating cells increases by 50% as seen in Fig. 6 (lower graph). Third, the length of the cells in the population increases dramatically by an average factor of 39% as seen in Fig. 2A. Finally, the ratio of the width of septating cells to the width of canoe cells is 1.20. During the more stressful conditions of transition and stationary phase, it thus appears that septating cells give rise to cells that are narrower than their parents. The same narrowing occurs again in stationary phase. This narrowing increases the SA/V; the average cellular SA/V increases by 22% for both transition and stationary phase cells.

Concluding thoughts

Our primary goal here has been presentation of thorough quantitative dataset of cellular shape in varying environmental conditions. We use the data to suggest a number of intriguing interpretations in the Discussion section. We hope the dataset and our suggestions will prove useful in developing questions about the mechanism of cellular shape control through future modelling.

Methods

Bacterium and culture conditions

The bacterium for all measurements was Acinetobacter baylyi strain ADP1 (also known as BD413) (4, 7). Strain ADP1 (BD413) was obtained from the American Type Culture Collection (strain 33305; Manassas, VA). The nonpolar min insertional knockouts were obtained from the French strain collection and crossed into the ATCC strain background by natural transformation (8).

For morphology over a growth curve experiments, cells were grown in Luria-Bertani (LB) broth (5 g yeast extract, 10 g tryptone, 10 g NaCl L^{-1}; also known as lysogeny broth) with high aeration at 25C or 37C (wild type cells). All data shown is from 37C growth conditions.

Mutant minC cells were grown at 30C in Minimal Davis Succinate broth.

For varying nutritional condition experiments, cells were grown in the following media at 37C: LB (same recipe as above), LB supplemented with ethanol (2 g/L = 43 mM), LB supplemented with glucose (0.4% = 22 mM), minimal M9 broth supplemented with ethanol (2 g/L = 43 mM), minimal M9 broth supplemented with 2,3-butanediol (5 mM), and minimal M9 broth supplemented with glucose (0.4% = 22 mM). Throughout the paper and figures these conditions are abbreviated as LB, LE, LG, ME, MB and MG respectively. Recipe for minimal M9 broth is as follows: 6 g Na2HPO4 dibasic, 3 g KH2PO4 monobasic, 0.5 g NaCl, 1 g NH4Cl dissolved in a final volume of 1 L deionized H2O, 2 mL 1 M MgSO4, and 100 ∝L 1 M CaCl. To make the overnight cultures prior to inoculating the final growth flasks, cells were grown in LB supplemented with the carbon source (ethanol (2 g/L = 43 mM), 2,3-butanediol (5 mM), or glucose (0.4% = 22 mM) matching the carbon source in the final growth flasks.

Growth curves

At time t_0, an overnight culture was diluted 1:1000 and incubated with high aeration. At regular intervals aliquots were processed to generate both the optical and number density curves simultaneously. All OD measurements taken at 600 nm using a standard spectrophotometer. For number density curves, 10 µL samples from a ten-fold dilution series were plated in triplicate on LB agar (1.5%) to determine CFUs/ml.

AFM sample preparation

The timing for making AFM samples for each experiment is as follows. For morphology over a growth curve experiments, the sampling time clock began when an overnight culture was diluted 1:1000. Culture was subsequently incubated with high aeration, and sampled every hour from 2–12 hours after inoculation. For minC experiments, mutant cells were grown until a growth curve showed they were in mid-exponential phase at which time it was sampled. For varying nutritional condition experiments, cells were also grown until they reached mid-exponential phase, at which time they were sampled.

For all experiments, at sampling time, an aliquot of culture was washed twice by gentle centrifugation and subsequently re-suspended in an equal volume of deionized, distilled, filter-sterilized water. On the final wash step, the cells were re-suspended in water adjusted to provide approximately 10^8 cells/mL. 15 µL was then applied to cleaved mica and allowed to air dry. Samples were imaged after air-drying for a minimum of 18 hours and stored at room temperature in sterile 12-well plates. We imaged air-dried cells

so that we could compare our cells to A. baumannii prepared the same way (20, 21). Air-drying without fixation also minimizes debris and the loss of surface structures such as pili associated with chemical fixation (30).

Controls

For control purposes we made, imaged, and analyzed numerous additional samples beyond what are shown in this paper. For morphology over a growth curve experiment, we made, imaged, and analyzed samples for three independent time series, two in which the bacteria were grown at 37 C and one in which the bacteria were grown at 25 C. The data shown are from one of the series at 37 C. For the mutant experiment, we studied multiple minC, minD, and minE samples as well as control wild type cells all grown under the same conditions; minD and minE mutants were substantially similar to minC (data not shown). For the varying nutritional condition experiments, we made four independent samples at each nutritional condition with a set of cells grown in LB made alongside in all cases.

AFM imaging

AFM images were obtained with a Bruker (formerly Digital Instruments and Veeco) MultiMode atomic force microscope, using silicon probes from Nanosensors type PPP-NCH or Bruker type NCHV-A, both with nominal spring constant 42 N/m and tip radius less than 10 nm. All images were obtained with tapping mode on desiccated samples in air at room temperature. The only image processing performed was a simple first order plane fit to correct for sample tilt. For all samples, we imaged in several disparate locations on a given sample.

AFM image analysis

Cell length and width measurements were obtained using the following procedures. All analysis was performed using Nanoscope Analysis software from Bruker.

Cell selection. For each AFM image, all cells were numbered and a random number generator was used to select 50 cells for measurement.

Length and Width Measurement. To measure a cell, we zoomed in on it in the topographic image, and then used the section to obtain a cross-section across the cell’s midline as shown in Fig. 1F. Cell boundaries were defined as the local minima between neighboring cells, as determined from the cross-section, with guidance from the topography to ensure the correct minima were chosen. Points defining either end of a cell were often at about the same elevation relative to the mica (Fig. 1F upper graph). In cases where one minimum was more than twice as deep as the other minimum (Fig. 1F lower panel), the shallower minimum was kept, while the opposite boundary was set such that it was of equal elevation to the shallower. If no local minimum could be found between two neighboring cells, inflection points in the topographic cross-section were used as boundary points. If no local minimum or inflection point could be found, the cell was skipped. Having identified the cell boundary points, the length and width were then defined as the horizontal distances between these defining points along the long and short axis respectively.

When they arose, two circumstances required special procedures for cell measurement. 1) Isolated cells. Cells were usually seen in clusters (Fig. 1). Given the size of the cantilever and usual cell spacing in clusters, typical local minima depths for clustered cells were 50–100 nm (Fig. 1F) because the cantilever was not small enough to reach the mica surface. To be consistent with measurements made for clustered cells, when measuring isolated cells, the cell dimension was defined using points set 50 nm below the cell surface, as opposed to measuring at its true minimum on the mica surface. 2) Cells where midline measurements were not appropriate. It would clearly be inappropriate to measure the width of bite or septating cells at their midline. In these cases, we simply moved the measurement away from the midline, often taking several measurements along the length of the cell to ensure we obtained a representative measurement.

Surface Area and Volume Calculations. Using a cell's dimensions, it is possible to calculate its surface area and volume and thereby also obtain its surface area to volume (SA/V) ratio. Since all cells are dried, height is not a good value to use in these calculations since cells primarily shrink in that dimension while preserving their length and width while drying (31). Also for clustered cells, absolute depth to the mica could not always be measured due to the size of the cantilever. Therefore, we assume that undried cells are rods with hemispherical end caps where the diameter of the sphere and rod are both given by the width. With l = length and w = width, the SA, V and SA/V ratio are calculated as:

$$\frac{SA}{V} = \frac{\pi w(\ell - w) + \pi w^2}{\frac{\pi w^2}{4}(\ell - w) + \frac{\pi w^3}{6}} = \frac{4\ell}{w(\ell - \frac{w}{3})}$$

Cell Type Classification. After a survey of images across a variety of population ages, five cell types were identified and strict quantitative criteria set forth to identify the types. Overall 62% of the cells in the entire time series were classified into one of these five types. The criteria for the types are outlined below.

1) Bite Cells. Bite cells possess a single deep, steep-sided feature that occurs midway along the cell's long axis. To qualify as a Bite, the feature must be deeper than 100 nm, comprise the sole significant feature on the cell surface, and occupy no more than two thirds of the cell's total length.

2) Divot Cells. Divot cells feature a pair of small depressions (divots) occurring on opposite ends of a cell's long axis. To qualify as divots, both depressions needed to exceed 10 nm in depth and measure at least 200 nm in both length and width. One additional central divot did not alter the classification of the cell; however, more than one additional divot or a non-central third divot disqualified the cell from the divot category.

3) Canoe Cells. Canoe cells possess a central surface depression that exceeded 10 nm in depth and was circumscribed by a higher, continuous ridge along the cell edge. To be classified as a canoe, it was required that the depression be continuous, run for at least half the cell's total length, and comprise the

sole significant feature on the cell's surface, with the exception of indentations that were occasionally found to occur at the bottom of the canoe's groove.

4) Smooth cells. Smooth cells are devoid of any significant surface features. A significant surface feature is defined as a symmetric feature that exceeds 10 nm in depth or any feature that exceeds 30 nm in depth.

5) Filament Cells. Cells are defined as filaments if their length exceeds 4 μm. The length criteria overrides all others, so even if their surface morphology meets the requirements for a different category, the cell was classified as a filament.

Septating Cells. Septating is not a cell type but rather is an additional classification that can be applied to any cell type. Candidate septating cells are identified from images as those with visibly constricting waists. Then both the width of the waist and the full width of the cell away from the waist were measured. The width of the cell was measured using the procedures outlined above. To ensure consistency, the endpoints for the waist measurement were then set at the same elevation as those of the width measurement. A septating cell was one that met the following criteria:

$$0.5 \leq \frac{waist\ width}{full\ width} \leq 0.9$$

Cells with a waist width below 50% of the full width are treated as independent cells.

References

1. Young KD: **Bacterial shape: Two-dimensional questions and possibilities.** 2010, *Annu Rev Microbiol* **64**:223-240.
2. Westfall CS, Levin PA: **Bacterial cell size: Multifactorial and multifaceted.** 2017, *Annu Rev Microbiol* **71**:499-517.
3. Elliott KT, Neidle EL: ***Acinetobacter baylyi* ADP1: Transforming the choice of model organism.** 2011, *IUBMB Life* **63**:1075-1080.
4. Juni E, Janik A: **Transformation of *Acinetobacter calcoaceticus* (bacterium anitratum).** 1969, *J Bacteriol* **98**:281-288.
5. TAYLOR WH, JUNI E: **Pathways for biosynthesis of a bacterial capsular polysaccharide. III. syntheses from radioactive substrates.** 1961, *J Biol Chem* **236**:1231-1234.
6. TAYLOR WH, JUNI E: **Pathways for biosynthesis of a bacterial capsular polysaccharide. I. characterization of the organism and polysaccharide.** 1961, *J Bacteriol* **81**:688-693.

7. Barbe V, Vallenet D, Fonknechten N, Kreimeyer A, Oztas S, et al: **Unique features revealed by the genome sequence of *Acinetobacter* sp. ADP1, a versatile and naturally transformation competent bacterium.** 2004, *Nucleic Acids Res* **32**:5766-5779.
8. de Berardinis V, Vallenet D, Castelli V, Besnard M, Pinet A, et al: **A complete collection of single-gene deletion mutants of *Acinetobacter baylyi* ADP1.** 2008, *Mol Syst Biol* **4**:174.
9. Dufrene YF: **Atomic force microscopy in microbiology: New structural and functional insights into the microbial cell surface.** 2014, *Mbio* **5**:e01363-14.
10. Dufrene YF: **Towards nanomicrobiology using atomic force microscopy.** 2008, *Nat Rev Microbiol* **6**:674-680.
11. Dufrene YF: **Using nanotechniques to explore microbial surfaces.** 2004, *Nat Rev Microbiol* **2**:451-460.
12. Dufrene YF: **Atomic force microscopy, a powerful tool in microbiology.** 2002, *J Bacteriol* **184**:5205-5213.
13. Brehm-Stecher BF, Johnson EA: **Single-cell microbiology: Tools, technologies, and applications.** 2004, *Microbiol Mol Biol Rev* **68**:538-59, table of contents.
14. Bolshakova AV, Kiselyova OI, Yaminsky IV: **Microbial surfaces investigated using atomic force microscopy.** 2004, *Biotechnol Prog* **20**:1615-1622.
15. Gaboriaud F, Dufrene YF: **Atomic force microscopy of microbial cells: Application to nanomechanical properties, surface forces and molecular recognition forces.** 2007, *Colloids Surf B Biointerfaces* **54**:10-19.
16. Auerbach ID, Sorensen C, Hansma HG, Holden PA: **Physical morphology and surface properties of unsaturated *Pseudomonas putida* biofilms.** 2000, *J Bacteriol* **182**:3809-3815.
17. Doktycz MJ, Sullivan CJ, Hoyt PR, Pelletier DA, Wu S, et al: **AFM imaging of bacteria in liquid media immobilized on gelatin coated mica surfaces.** 2003, *Ultramicroscopy* **97**:209-216.
18. Beckmann MA, Venkataraman S, Doktycz MJ, Nataro JP, Sullivan CJ, et al: **Measuring cell surface elasticity on enteroaggregative *Escherichia coli* wild type and dispersin mutant by AFM.** 2006, *Ultramicroscopy* **106**:695-702.
19. Steinberger RE, Allen AR, Hansa HG, Holden PA: **Elongation correlates with nutrient deprivation in *Pseudomonas aeruginosa*-unsaturates biofilms.** 2002, *Microb Ecol* **43**:416-423.
20. Soon RL, Nation RL, Cockram S, Moffatt JH, Harper M, et al: **Different surface charge of colistin-susceptible and -resistant *Acinetobacter baumannii* cells measured with zeta potential as a function of growth phase and colistin treatment.** 2011, *J Antimicrob Chemother* **66**:126-133.
21. Soon RL, Nation RL, Hartley PG, Larson I, Li J: **Atomic force microscopy investigation of the morphology and topography of colistin-heteroresistant *Acinetobacter baumannii* strains as a function of growth phase and in response to colistin treatment.** 2009, *Antimicrob Agents Chemother* **53**:4979-4986.
22. Margolin W: **Sculpting the bacterial cell.** 2009, *Curr Biol* **19**:R812-22.

23. Corbin BD, Yu XC, Margolin W: **Exploring intracellular space: Function of the min system in round-shaped *Escherichia coli*.** 2002, *Embo j* **21**:1998-2008.
24. Vallenet D, Nordmann P, Barbe V, Poirel L, Mangenot S, et al: **Comparative analysis of *Acinetobacters*: Three genomes for three lifestyles.** 2008, *PLoS One* **3**:e1805.
25. Reichert B, Dornbusch AJ, Arguello J, Stanley SE, Lang KM, et al: ***Acinetobacter baylyi* long-term stationary-phase protein StiP is a protease required for normal cell morphology and resistance to tellurite.** 2013, *Can J Microbiol* **59**:726-736.
26. Nystrom T: **Stationary-phase physiology.** 2004, *Annu Rev Microbiol* **58**:161-181.
27. Yu XC, Margolin W: **FtsZ ring clusters in min and partition mutants: Role of both the *min* system and the nucleoid in regulating FtsZ ring localization.** 1999, *Mol Microbiol* **32**:315-326.
28. Adams DW, Errington J: **Bacterial cell division: Assembly, maintenance and disassembly of the Z ring.** 2009, *Nat Rev Microbiol* **7**:642-653.
29. Fenton AK, Gerdes K: **Direct interaction of FtsZ and MreB is required for septum synthesis and cell division in escherichia coli.** 2013, *Embo j* **32**:1953-1965.
30. Chao Y, Zhang T: **Optimization of fixation methods for observation of bacterial cell morphology and surface ultrastructures by atomic force microscopy.** 2011, *Appl Microbiol Biotechnol* **92**:381-392.
31. Trueba FJ, Woldringh CL: **Changes in cell diameter during the division cycle of *Escherichia coli*.** 1980, *J Bacteriol* **142**:869-878.

Supporting Information

S1 Guide to data files submitted with *Quantitative atomic force microscopy measurements of bacterial morphology*. This document provides an overview of the two excel files containing the data submitted with this paper.

S2 Dataset for bacterial morphology over a growth curve. This dataset contains morphology data for cells at regular intervals during a growth curve. This dataset was used to make Figures 2, 3, 4, 6 and 7. The images in Figures 1 and 5 were drawn from images analyzed in this dataset.

S3 Dataset for bacterial morphology in varying nutritional conditions. This dataset contains morphology data for cells grown in varying nutritional conditions. This dataset was used to make Figures 9 and 11. The image in Figure 10 is drawn from images analyzed in this dataset.

Declarations

- Ethics approval and consent to participate: not applicable (no human subjects)
- Consent for publication: not applicable (no human subjects)
- Competing interests: The authors declare that they have no competing interests.

- Funding: This research was made possible by grant support from the National Science Foundation Biology Directorate (MCB-1330511, Lang & Lostroh). The funders had no role in study design, data collection and analysis, decision to publish, or preparation of the manuscript.
- Authors' contributions: CM, NL, KR, SW, WM, and AB-M were responsible for data acquisition and analysis. CPL and KL are responsible for the conception and design of the work; the interpretation of data; and drafting the manuscript. All authors have approved the submitted version and have agreed to be personally accountable for their own contributions and to ensure that questions related to the accuracy or integrity of any part of the work, even ones in which the author was not personally involved, are appropriately investigated, resolved, and the resolution documented in the literature.
- Acknowledgements: We gratefully acknowledge the work of several students who took preliminary data and contributed to our understanding of these topics broadly including Andrew Shum, Samuel Zemedkun, Melody Maxson, Nathan Gustilo, Amber Dornbusch, Ricardo Tenente and all the students in our biophysics seminars.

Data availability

The datasets (images) during analyzed during the current study available from the corresponding author on reasonable request. The quantitative measurements of those datasets are included as supplementary materials.

Figures

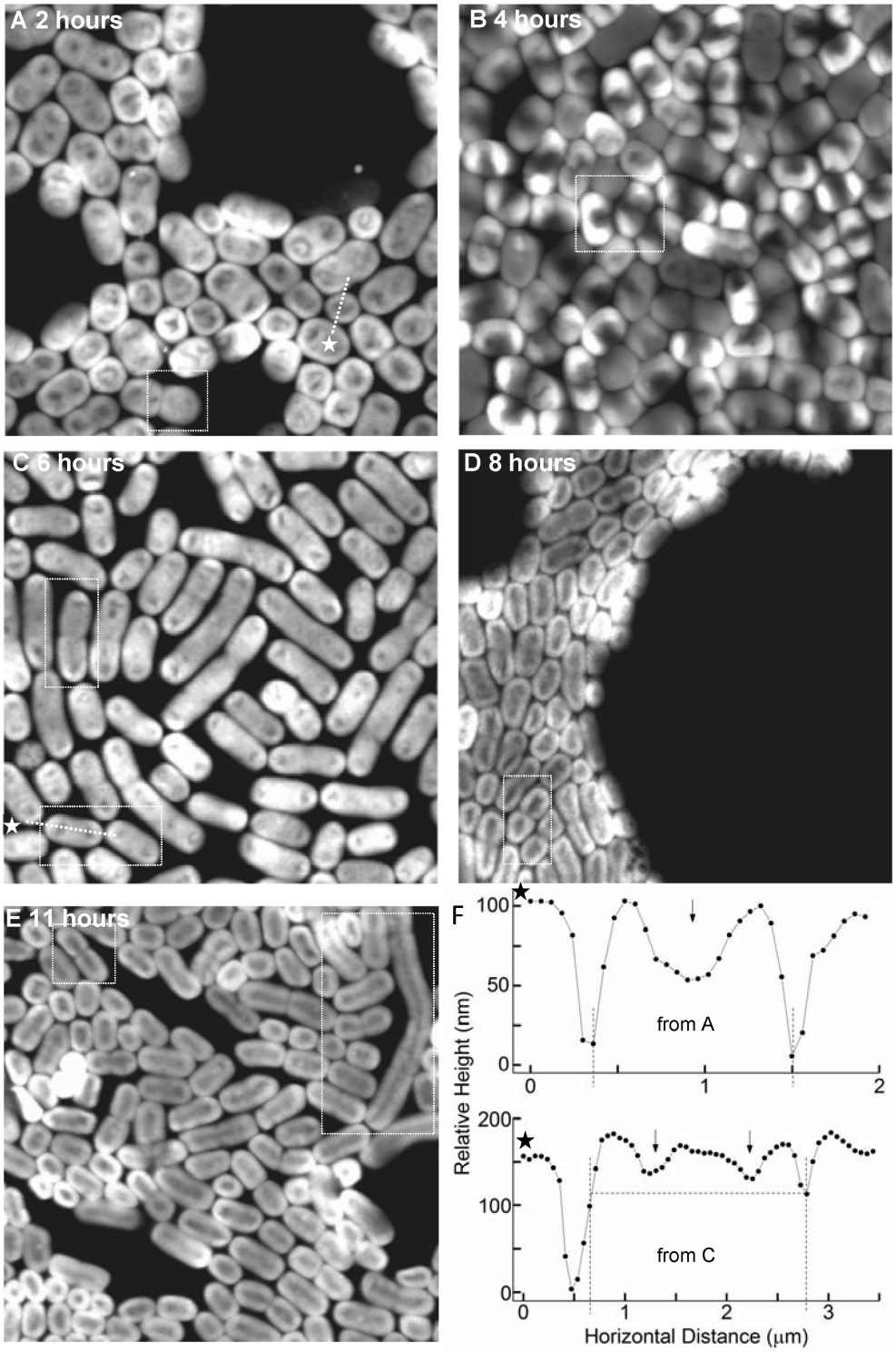

Figure 1

AFM topographs displaying bacterial morphological changes during a growth curve. All images are 15 μm x 15 μm and were obtained at population age A) 2 hours, B) 4 hours, C) 6 hours, D) 8 hours and E) 11 hours after inoculation. The only image post-processing performed was a simple first order plane fit. The boxed cells in each image are described in the text and presented in Fig 4 in three-dimensional close-ups. Panel F shows cross-sections from panels A and C in the upper and lower graphs respectively. These

cross-sections demonstrate the three-dimensional nature of AFM data and illustrate how cell length is measured. The star on an image and its corresponding cross-section are at about the same position. For the upper graph in Panel F, the cell length is defined as the distance between the two local minima at the cell's end, as marked by the dashed lines, yielding a length of 1.14 μm for this cell. For the lower graph in Panel F, the local minima differ significantly in height, so here the cell length is defined as the distance between the shallowest local minimum and the equal height location on the opposite side of the cell, as marked by the dashed lines, yielding a length of 2.14 μm.

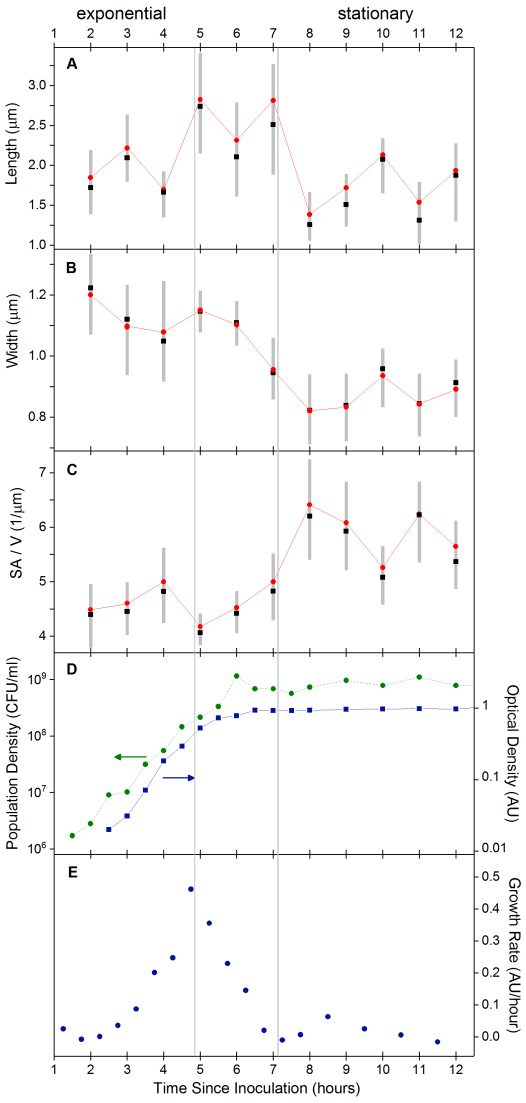

Figure 2

Quantitative changes in bacterial morphology during a growth curve. Average A) length, B) width, and C) surface area to volume ratio for the cell population at a given time after inoculation. Surface area (SA) and volume (V) of cells were calculated from primary measurements assuming cells were rod shaped with hemispherical end caps. In all panels the red circles plot the mean and the black squares plot the median. The gray bars show the size of the 25th to the 75th percentiles of the population. D) Bacterial growth curves obtained using dilution plating (green) and optical density (blue). The optical density curve is used to plot the growth rate given in E). Taken together, the growth curve and growth rate indicate the population is in exponential phase from hours 2 – 4 after inoculation, in transition in hours 5 – 7, and in stationary phase in hours 8 and beyond. The time periods are indicated by the vertical gray lines.

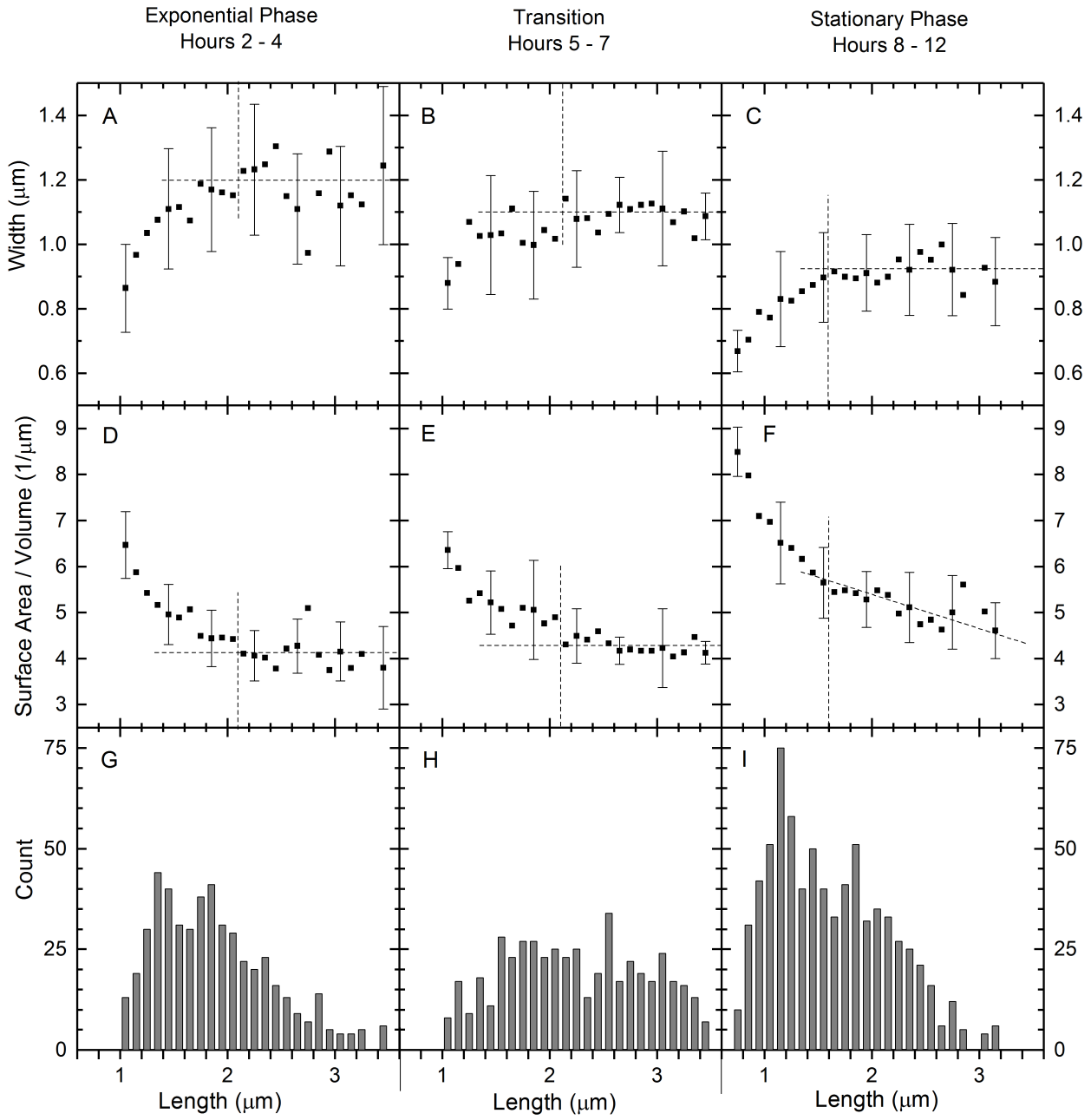

Figure 3

Cell width, SA/V, and counts as a function of length. Population is split into cells in exponential phase (hours 2 – 4), transition (hours 5 – 7) and stationary phase (hours 8 - 12). Within each time period, plots are average width (A, B, C respectively), average surface area to volume (D, E, F), and cell counts (G, H, I) for cells in given length ranges. The error bars give the standard deviation of the measurements in a given length range. Only a selection of error bars is shown since they are all comparable in size within a given panel. Width and SA/V averages representing fewer than four cells are omitted.

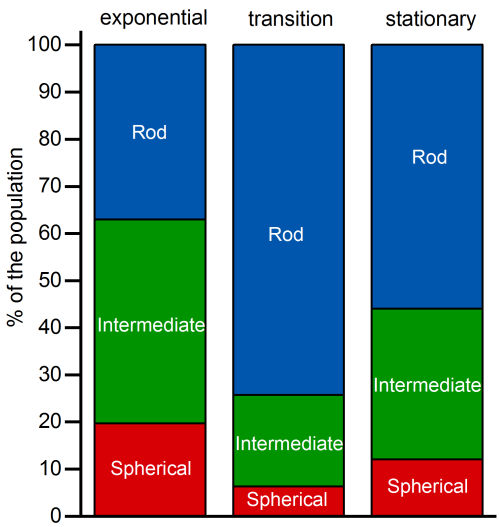

Figure 4

Cell shape distribution during different periods of the growth curve. Population is split into cells in exponential phase (hours 2 – 4, N= 508), transition (hours 5 – 7, N =591) and stationary phase (hours 8 – 12, N = 783). Within each period the length to width (aspect) ratio for all cells is found. Cells with aspect ratio ≤ 1.25 are deemed spherical, cells in the range where 1.25 < aspect ratio ≤ 1.75 are deemed intermediate, and cells where aspect ratio > 1.75 are deemed rods.

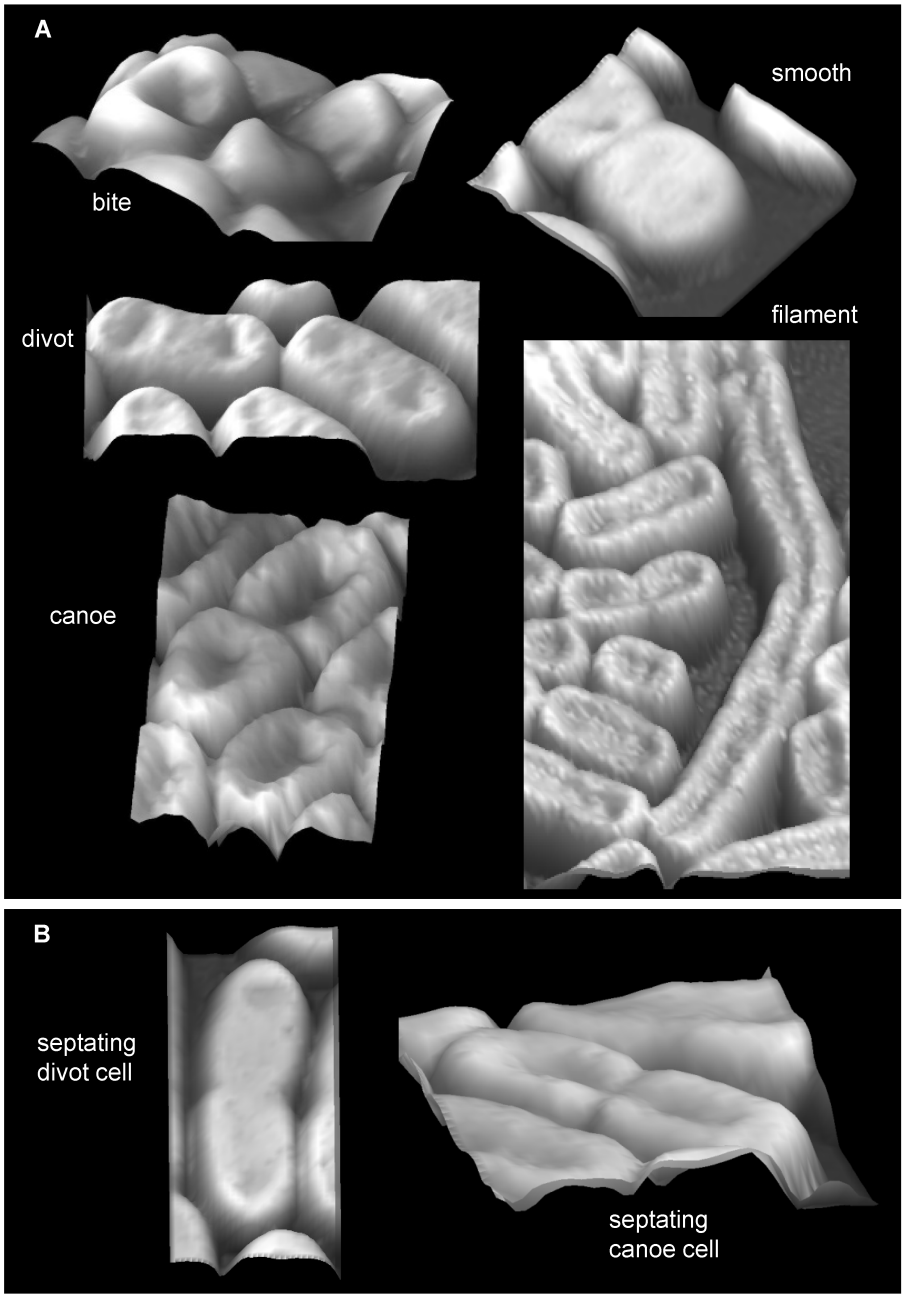

Figure 5

Close-up topographs of identified cell types and of septating cells. A) The five three-dimensional images show cell types in detail and are cropped from the larger images of Fig 1, which thereby gives the length scale for each image. The bite cells are cropped from 1B, the divot cells from 1C lower left, the canoe cells from 1D, the smooth cell from 1A, and the filament cell from 1E. B) Detail of septating cells. Cells on left and right are cropped from Fig 1C (mid-left) and 1E (upper left) respectively.

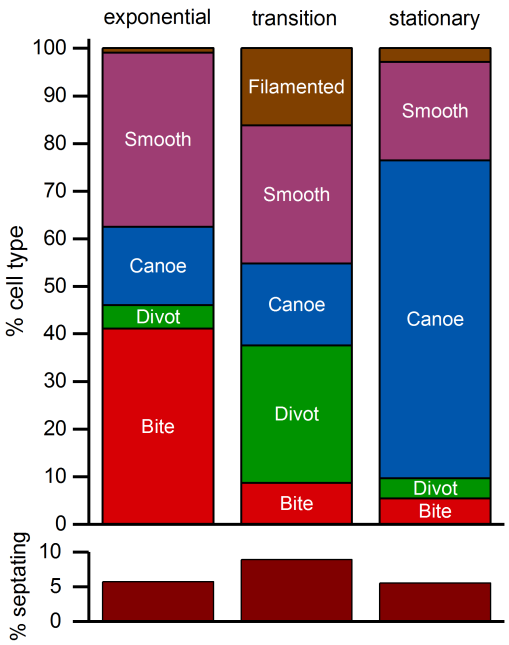

Figure 6

Relative frequency of occurrence for cell types over a growth curve. The upper graph shows the relative frequency of occurrence for the five cell types identified in Fig 5A during exponential phase (hours 2 – 4 after inoculation), the transition (hours 5 – 7), and stationary phase (hours 8 - 12). The lower panel gives the percentage of cells observed to be septating during those same three time periods.

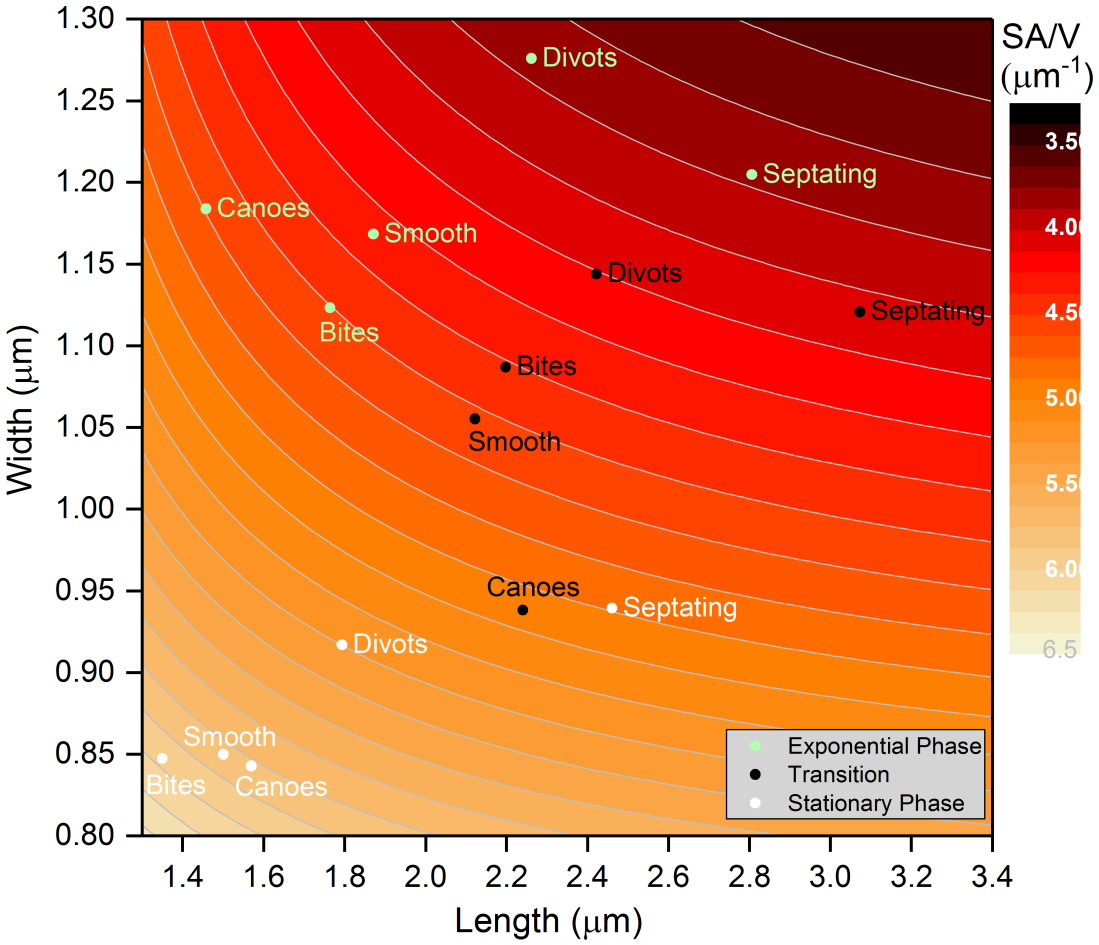

Figure 7

Length, width and SA/V for cell types over a growth curve. Each point on the graph shows the average length and width for a given cell type during exponential phase (green), transition (black), and stationary phase (white). The background color shows the SA/V given the average length and width and assuming cells are rod shaped with hemispherical end caps. We now focus on the vertical axis of Fig 7 to examine trends in the width of cell types. In exponential phase, canoes and smooth cells have similar widths with bites a bit narrower, whereas divots and septating cells are wider. During the transition from exponential phase to stationary phase, all the cell types have narrower widths. Bites and smooth cells have similar widths, again with divots and septating cells wider. However, now the canoes are very narrow as compared to all other cells during this time. In stationary phase, all the cell types have again shifted to lower widths. A similar pattern holds regarding the relationships between cell types- bites, smooth and canoes are the narrowest cells, with divots and septating cells wider.

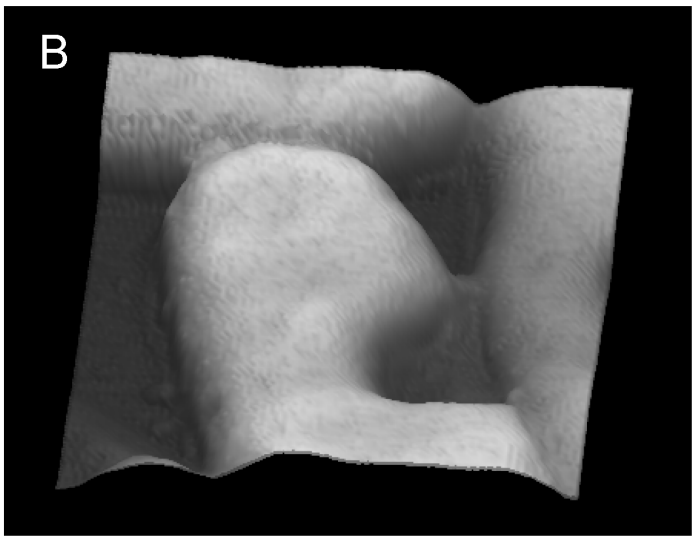

Figure 8

AFM topographs of minC mutant of A. baylyi. A) 15 μm x 15 μm image taken of minC mutant cells during exponential phase. The only image post-processing performed was a simple first order plane fit. B) Three dimensionally rendered close-up of the region boxed in Panel A. Fig 8A shows that the minC mutant consists mostly of filamented cells, as expected because minicells likely wash away during sample preparation. Along the length of these filaments are indentations that can be compared to those observed

in wild type cells shown in Fig 1B. Zooming in on the boxed cell in Fig 8A, in Fig 8B we show a close-up of the one of the indentations, which can be compared to the close-up bite cells in Fig 5A.

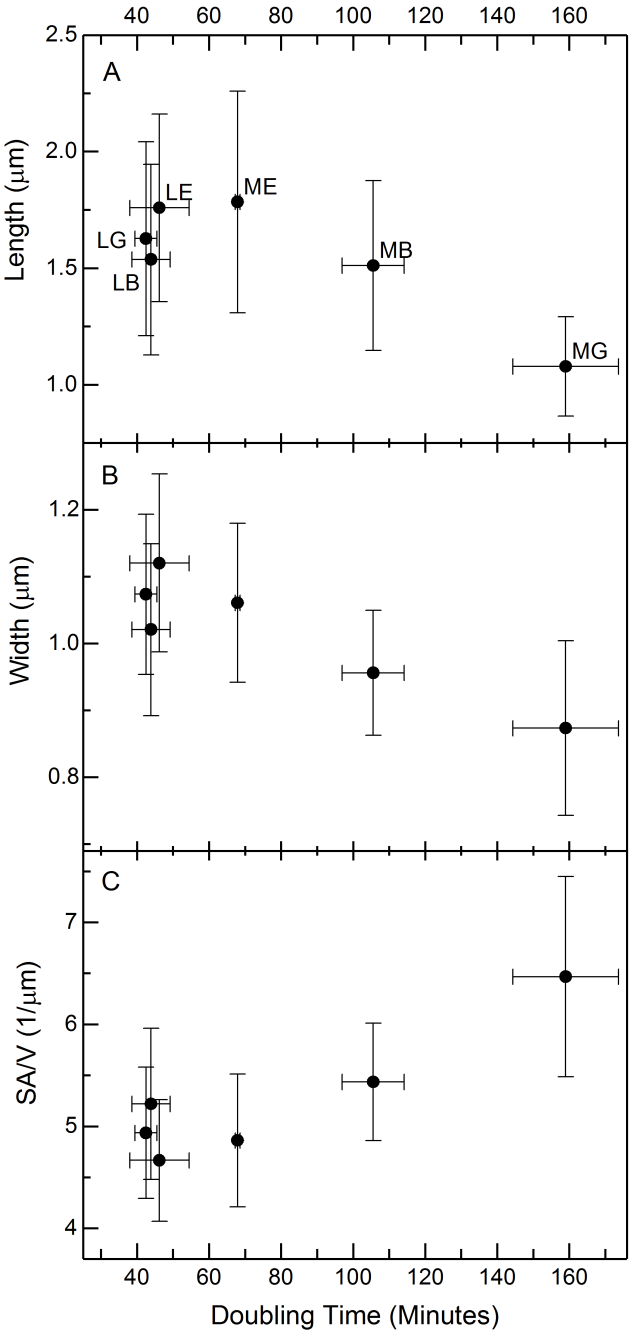

Figure 9

Quantitative changes in bacterial morphology for cells grown in media with varying doubling time. For the x axis, the doubling time for a given medium is obtained by fitting the exponential phase points of a growth curve. Multiple times thus obtained from independent growth curves are averaged, and the error

bars give the standard deviation. Against this x value is plotted the average A) length B) width and C) surface area to volume ratio for the cell population grown in those media. Y-error bars give the standard deviation of cellular measurements. Surface area (SA) and volume (V) of cells were calculated from primary measurements assuming cells were rod shaped with hemispherical end caps.

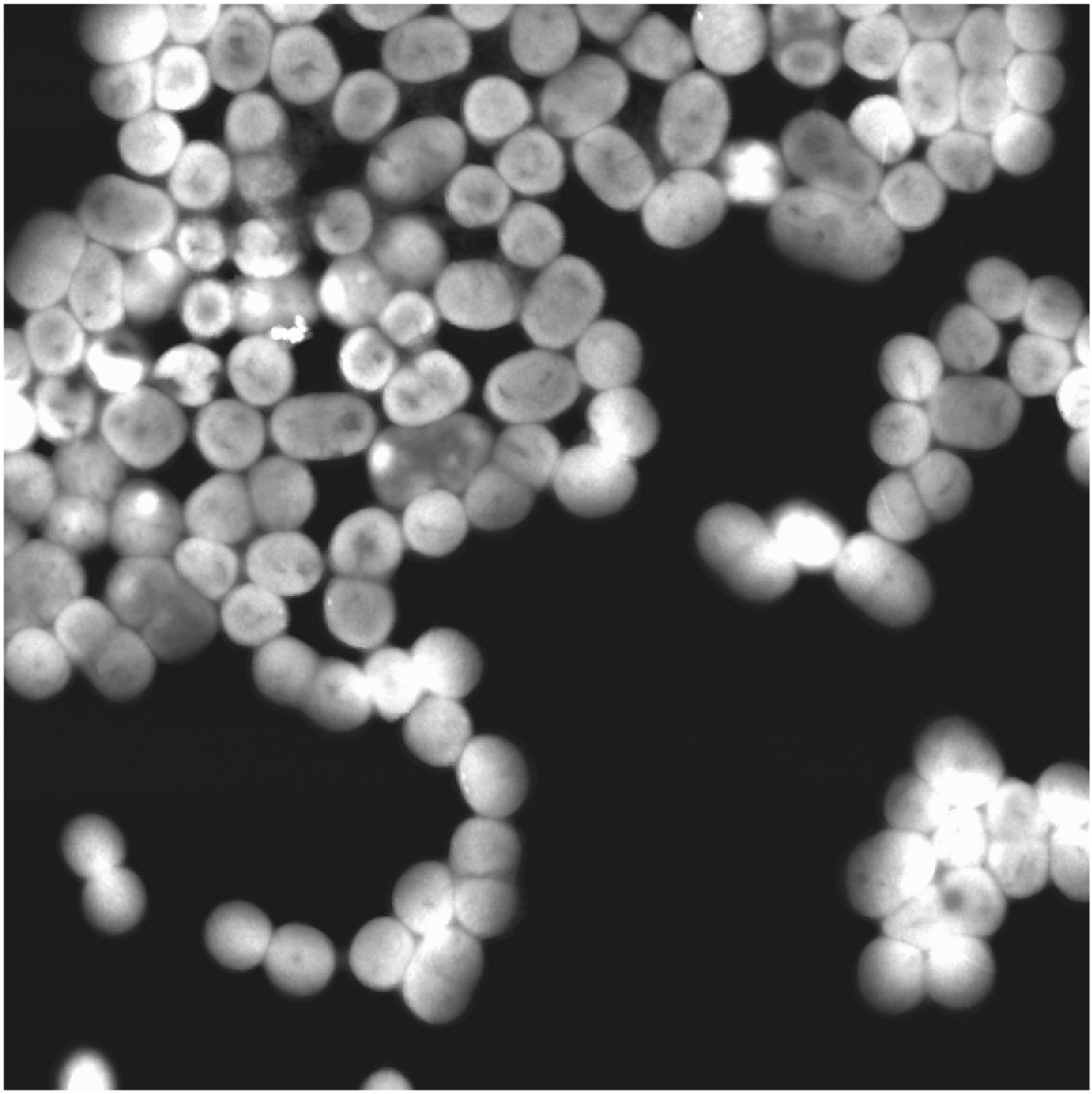

Figure 10

AFM topograph of exponential phase cells grown in minimal medium with glucose (MG). Image is 15 µm x 15 µm. The only image post-processing performed was a simple first order plane fit.

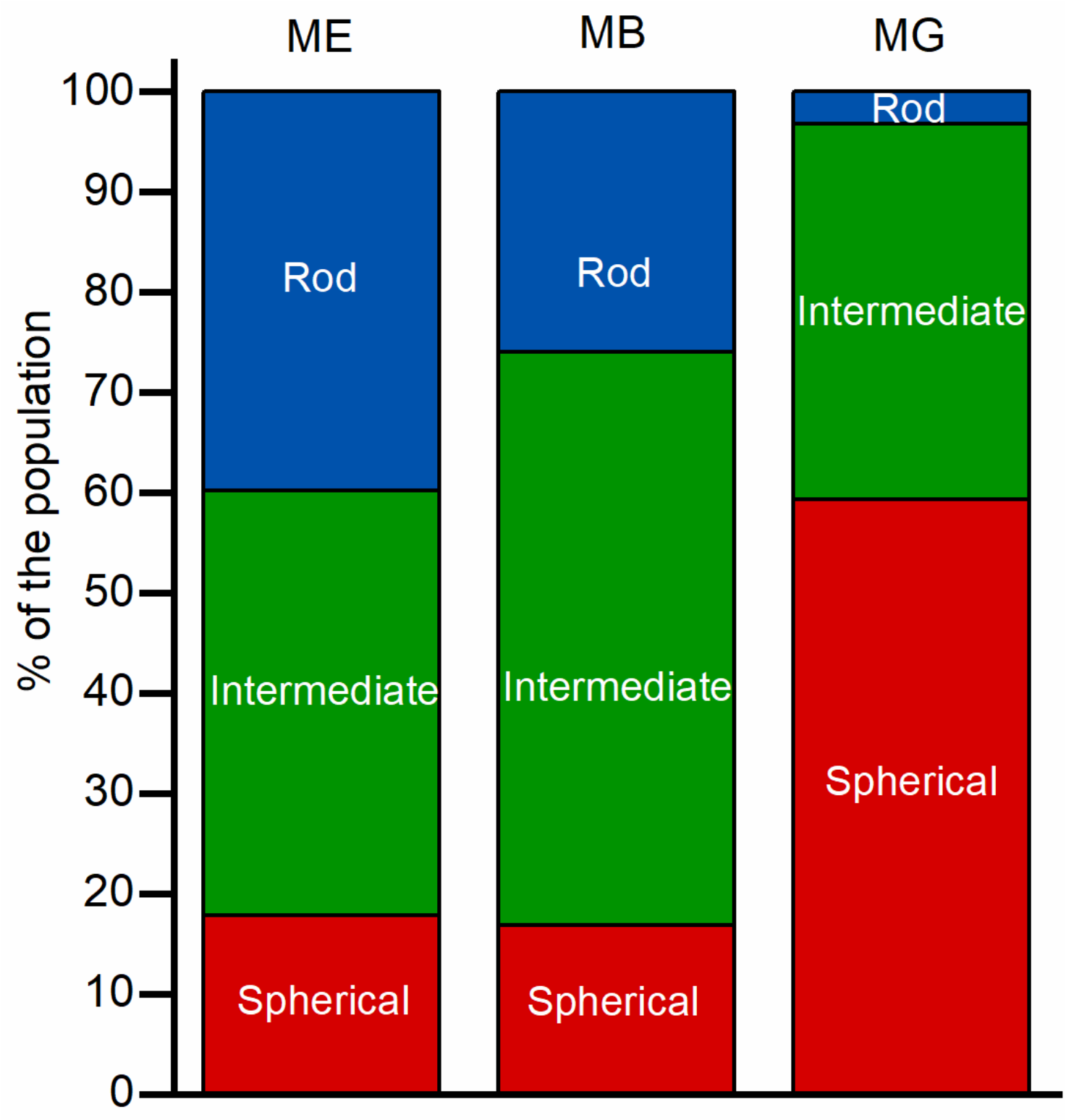

Figure 11

Cell shape distribution for cells grown in minimal media with differing additives. For minimal medium: with ethanol (ME) N = 314; with 2-3 butanediol (MB) N = 308; with glucose (MG) N = 310. For each medium, the length to width (aspect) ratio for all cells is found. Cells with aspect ratio ≤ 1.25 are deemed spherical, cells in the range where 1.25 < aspect ratio ≤ 1.75 are deemed intermediate, and cells where aspect ratio > 1.75 are deemed rods.

Supplementary Files

This is a list of supplementary files associated with this preprint. Click to download.

- Datasetformorphologyinvaryingnutritionalconditions.xlsx
- Guidetodatafilessubmitted.docx
- Datasetformorphologyoveragrowthcurve.xlsx